International Journal of Advances in Electrical Engineering

E-ISSN: 2708-4582
P-ISSN: 2708-4574
IJAEE 2025; 6(1): 77-82

www.electricaltechjournal.com
Received: 10-02-2025
Accepted: 15-03-2025

Nasreen Taj M
Department of Electrical and Electronics Engineering, Sri Siddartha Institute of Technology, Sri Siddartha Academy of Higher Education (SSAHE), Tumakuru, Karnataka, India

Correspondence Author:
Nasreen Taj M
Department of Electrical and Electronics Engineering, Sri Siddartha Institute of Technology, Sri Siddartha Academy of Higher Education (SSAHE), Tumakuru, Karnataka, India

Optical and electrical properties of molybdenum oxide nanoparticles for super capacitor applications

Nasreen Taj M

DOI: https://www.doi.org/10.22271/27084574.2025.v6.i1a.90

Abstract
Molybdenum oxide nanoparticles (MoO_3 NPs) were prepared by the ultrasonication method using a surfactant. Prepared samples exhibited a hexagonal form with excellent crystallite form, without any impurities, as observed from the powder X-ray diffraction technique. Rod-like structures with various layers were observed from the SEM images, which is the characteristic nature of MoO_3 NPs. With the use of surfactant, the agglomeration was reduced. Energy bandgap obtained from UV-Visible spectrograph, the E_g value was increased from 3.24 to 3.26 eV in the presence of surfactant. Super capacitor studies were performed by using Cyclic Voltammetry showed that the prepared samples are suitable for enhancing the efficiency of electrodes by coating them with these nanoparticles. The performance was confirmed by observing the enhanced specific capacitance and the charging-discharging curves. Hence, the prepared samples are useful in designing advanced super capacitors that can replace the existing lithium-ion batteries and capacitors.

Keywords: Nanoparticles, super capacitors, luminescence, specific capacitance

Introduction
Supercapacitors (SCs) have emerged as a viable strategy in the search for alternative energy storage devices because of their stability, areal capacitance [1], high power density, low energy density, affordability, long cycle life, and ecologically benign operations [2]. SCs, also known as electrochemical capacitors, are energy storage devices that bridge the gap between traditional capacitors and batteries by offering high capacitance values and rapid charge/discharge capabilities, outstanding specific power (greater than 10 $kWkg^{-1}$) [3]. Super capacitors offer significantly higher power density compared to conventional capacitors, enabling rapid charge and discharge cycles, which is essential for applications requiring quick bursts of energy. SCs are classified into three distinct groups, namely, electric double-layer capacitors (EDLCs), pseudocapacitors (PCs), and hybrid capacitors. In the design of super capacitors, the active material plays a crucial role in determining their electrochemical performance.

Among different metal oxides, MoO_3 is inexpensive, non-toxic, and serves as an efficient and exhibiting better properties. MoO_3 NPs have been the emphasis due to their notable intercalation chemistry. Their exceptional properties are useful for numerous engineering applications, *viz*., sensors, photochromic, electronic display materials, and devices [4-6]. It exists in three crystal phases, among them the orthorhombic phase is thermodynamically more stable, while the monoclinic and hexagonal forms are metastable. In the orthorhombic phase, two-dimensional layers are stacked to have two sub-layers in the (010) direction [7]. The tunnel of charge carriers through the connected network helps for electron-hole pair separation under irradiation and enhances the photochromic performance [8], batteries [9], white LEDs, etc. [10]. In addition, MoO_3 show polymorphism; hence, it exhibits different morphologies *viz*., nanofibers, nanorods, and nanowires, useful for various applications. Optical properties of MoO_3 NPs can be achieved by controlling their morphologies and phases, which in turn helps in sensing the excitation light source [11]. Multi-hole structures, generally with plentiful cavities, could enhance light harvesting from multiple light reflections and scattering in-between the cavities. Chen [12] and Huang [13] effectively synthesized MoO_3 hexagonal prisms, but with hexagonal prisms photochromic property reduced. Also, Yao [14] reported that MoO_3 nanofibers produced by the hydrothermal method decreased, and the nanofibers always have with large exposed surface area [15].

The performance of the sample is improved.

Various methods were proposed for the MoO_3 NPs preparation, to name a few, hydrothermal [16] and microwave [17], Solution combustion, etc., are soft chemistry routes. Here, a sonochemical method is used to synthesize MoO_3 NPs with controllable morphologies. In this method, the solution, when subjected to sonochemical treatment, has many advantages; (i) the ultrasonic excitation can give a short duration of extremely high temperature at highly localized spots in the liquid phase to facilitate the reaction, (ii) It is simple and conducted in aqueous solution which can be easily implemented in large scale production. (iii) Morphologies of the NPs can be controlled by tuning the acidity of the coordinating solution.

Experimental

Precursors taken for the synthesis are of a stoichiometric amount of ammonium heptamolybdate tetrahydrate (AHM). It was added to a 75 ml mixture of de-ionized (DI) water, 10% diluted hydrochloric (HCl) acid, and ethanol. As a surfactant, Cetyltrimethylammonium bromide [CTAB; 1 g] was used during the preparation to bring changes in the morphology. This mixture was sonicated for a few minutes to get a clear solution. Then the solution was transferred to an ultrasonic bath and agitated at 180 °C for 1 h. The solution turned into a light-blue precipitate was centrifuged and washed with DI water and ethanol several times. Finally, ∝-MoO_3 NPs were obtained after heating the sample in a vacuum at 60 °C for 16 h. The morphologies were changed from soft agglomeration to rod shape, strong and stable compound, by changing the HCl concentration from 5% to 15%.

Results and Discussions

Fig.1 shows the powder X-ray diffraction (PXRD) patterns of MoO_3 NPs synthesized at 600 °C using the ultrasonication method with different HCl concentrations of 15%, 10%, and 5%. The hexagonal structure of MoO_3 with JCPDS No. 29-0115. The purity of the samples was because of the influence of the chemical reaction pathway, nucleation, and growth of the resultant products due to the increased concentration of HCl. In general, the rise in the concentration allows the crystallite to nucleate, grow along specific growth sites, and arrange orderly, thus promoting high crystalline samples with increased crystallite size.

Morphological behavior of MoO_3.

The morphology was studied for 600 ^oC heated samples for different concentrations of HCl in the presence of 1g CTAB, and the results are shown in Fig. 2. It was observed that the sample exhibits hexagonal-shaped nanorods. All atoms of these individual rods were at high energy, leading to the vibration and diffusion process. The strength of vibration and diffusion of the solid was controlled by the calcination temperature, bond strength, and type of bonds. It can be noted that, as shown in Fig. 2a to 2c, the morphologies of h-MoO_3 changed to a rod-like shape by increasing the acidity of the solution from 5% to 10% and 15% HCl at the same reaction temperature. Upon sonication, H_2MoO_4 would dehydrate and form numerous MoO_3 NPs, which could serve as the nuclei. The formation mechanism of hierarchical of this microstructures of can be explained in successive stages like: (i) homogeneous nucleation of h-MoO_3 via dissociation and association of precursors at a controlled reactant species, concentration and the type of a solvent medium (ii) self-assembly process for the formation of anisotropic growth of hexagonal phase MoO_3 nuclei (iii) evaluation of 1D hexagonal rods through Ostwald ripening. By increasing the sonication time, the particle surfaces were destroyed and tended to dissolve the particles. This results in breaking up the balance between individual rods with the increased concentration of the precursors. This was due to the increased kinetic and thermodynamic energy. Thus, the appropriate reaction temperature and time provide sufficient energy input to promote the reactants' speed and strong attractive interactions, resulting in controlled nucleation and growth towards well-developed hierarchical rod-like microspheres. The TEM images shown in Fig. 3(a) show the presence of both short and long-sized rods, but all are in the nano-regime. They were highly dense and agglomerated and were mixed with particles, thus resulting in non-uniform dispersibility. Fig. 3b shows the HR TEM with the interplanar spacing of 0.327 nm. Fig. 3c confirms the SAED pattern with the polycrystalline nature, and Fig. 3d shows the sample purity of only MoO_3 NPs without any impurity elements.

Optical Energy gap determination using UV-Visible spectrometer: The optical characterization of prepared samples was carried out by diffusion reflectance spectroscopy (DRS) spectra recorded in the wavelength range from 300 - 700 nm (Fig. 4a). Spectra show a strong reflectance response between 420 - 570 nm, which indicates the high absorption in the visible region. The visible absorption was the characteristic optical absorption of h-MoO_3 due to vacant “d” orbitals of the cation (Mo^{6+}) and “p” orbitals of the oxygen atoms with a lone pair of electrons (O^{2-}). Kubelka-Munk relation was used to correlate the diffused reflectance to the absorption coefficient. In this case, the Kubelka-Munk equation at any wavelength becomes [18].

$$F(R) = \frac{(1-R)^2}{2R} \text{ - - - - - (1)}$$

Where R; the absolute reflectance of the sample and F(R); the so-called Kubelka-Munk function. The diffused reflectance for all the samples increased with increasing wavelength. The optical band gap of phosphors exhibits the fundamental absorption, which corresponds to electron excitation from the valance band to conduction band and determined by the following relation $(F(R)\ h\upsilon)^n = A(h\upsilon - E_g)$, where n = 2 for a direct allowed transition, and n = 1/2 for an indirect allowed transition, A is the constant, and hυ is the photon energy [19]. The linear part of the curve was extrapolated to $(F(R)h\upsilon)^{1/2} = 0$ to get the indirect band gap energy. The E_g found to be 3.6 eV to 3.4 eV for different concentrations of HCl due to the reduced crystallite size

Figure 5 shows the PL spectra of MoO_3 prepared at 15% concentration of HCl at an excitation wavelength of 324 nm. All three samples show strong emission between 400-600 nm. The emission spectra show a strong peak positioned at 438 nm can be due to the hexa-coordinated $[MoO_6]^{5+}d_z^{2-}d_{yz}$ transitions and show stronger emission at a lower wavelength (438 nm). Such an enhancement in PL intensities is possible due to a decrease in grain size or an increase in specific surface area. The change in PL intensities is regular; for instance, at 600 ^oC has the highest

emission intensity. The results mean that the processing procedures of MoO_3 crystals, including sintering temperatures and times, have a direct effect on their PL intensities.

Cyclic Voltammetry and the supercapacitor studies

The prepared samples were used as an electrode material. Nickel foam of 0.25 mm^2 area was taken and coated with MoO_3 NPs. After the coating of 0.3 mg of samples, the electrode was heated and washed to remove the excess NPs. Potassium hydroxide (KOH) solution was used as an electrolyte and platinum was used as a counter electrode. The cell was connected to the cyclic voltameter and studied the I-V characteristics, GCD (Galvonic Charge Discharge) and EIS studies were performed. The separator used is a poly-paraffin sheet, which is more stable in the liquid environment and also provides the necessary pores for the ions to exchange between the anode and cathode regions. Fig. 6 shows the CV characteristics of all the three samples for various voltages from 5 mV/s to 50 mV/s. Among them the area under the curve is highest for HCl of 15% which has the highest specific capacitance. A three-electrode configuration was used to examine the electrochemical performance. It showed from Fig. 6 and 7 a maximum specific capacitance C_s of 991 Fg^{-1} at 5mVs^{-1} for 15% HCLl concentration among the three cases. This is due to its uniformly distributed nanostructured morphology with high porosity and an enhanced surface-to-volume ratio. Fig. 8 shows the GCD curves are also presented to investigate the electrochemical characteristics of the composites. The potential ranges from -1 V to 0.5 V at different current rates of 1 mA to 5 mA. The potential time response of these curves presents a non-linear curve, originating from Faradic behavior. It is a fundamental feature of battery-type materials, as mentioned in CV analysis. At lower current rates, electrochemical reactions occur in a more stable and regulated fashion, which results in a narrower potential window because of the slower and more complete usage of the active electrode. As the current rate rises, faradic reactions gain more significance, providing elevated potentials to maintain charge transfer rates

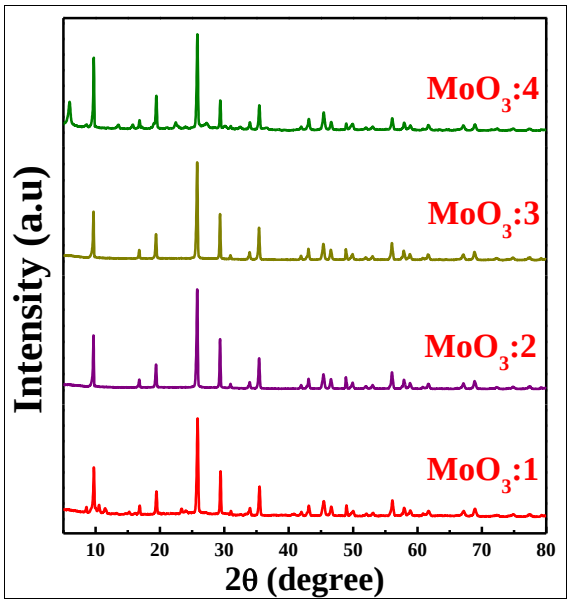

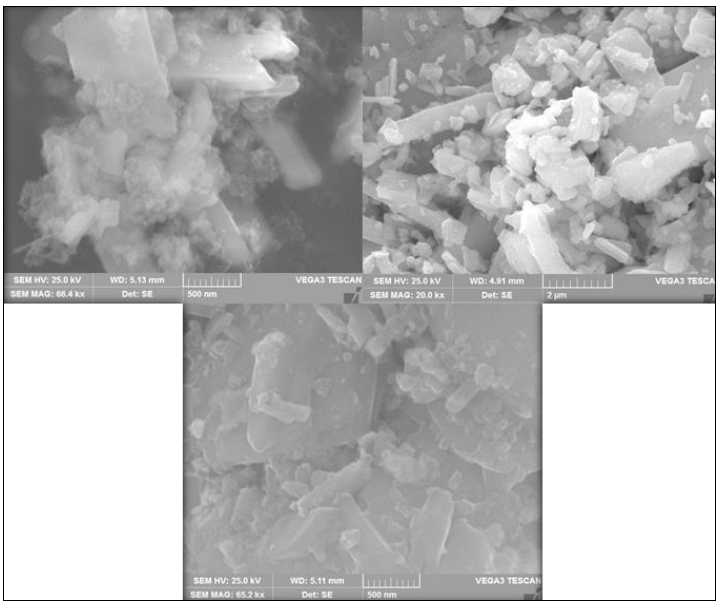

Fig 1: PXRD pattern for the MoO_3 NPs with different AV gel concentrations. **Fig 2:** SEM Images of MoO_3:1, 2 and 3 samples.

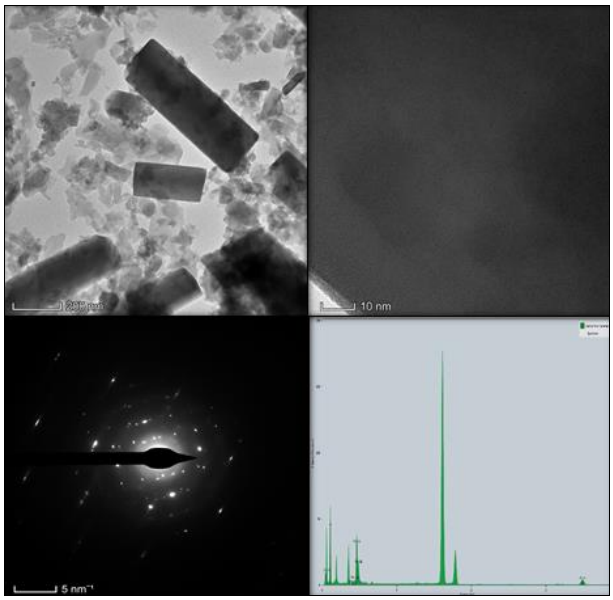

Fig 3: (A) TEM image, (B) HR TEM image, (C) SAED pattern, and (D) EDX of the MoO3:3, which has the better specific capacitance.

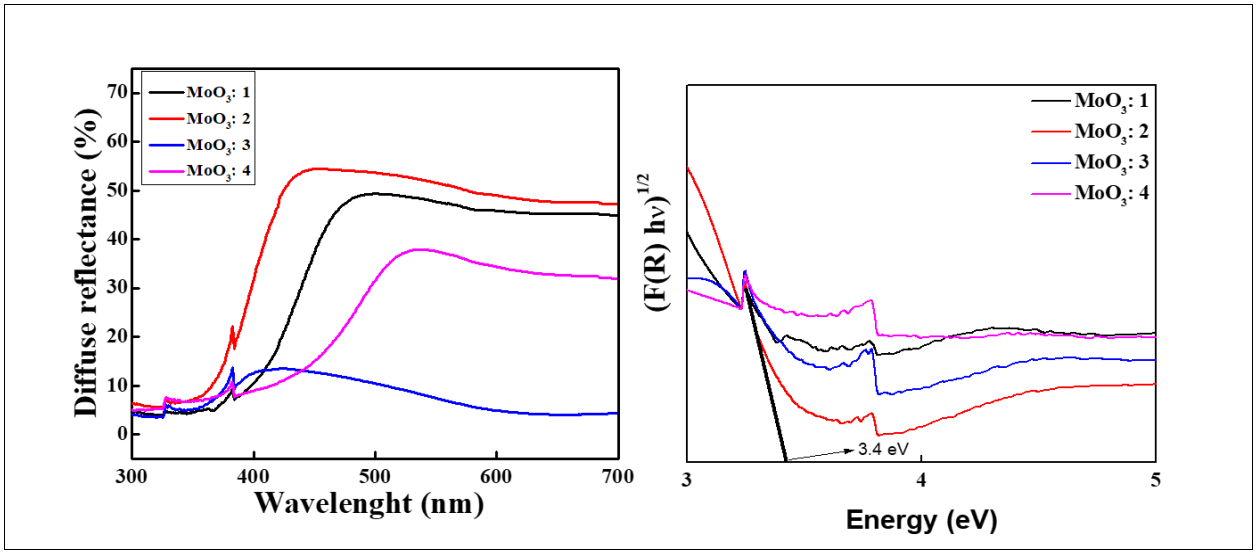

Fig 4: UV-Vis spectra of MoO3 NPs. All have almost the same energy band gap.

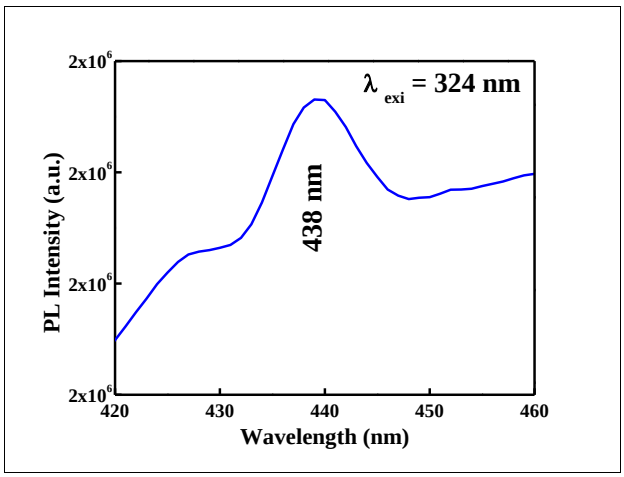

Fig 5A: PL emission spectra of MoO3:3 excited at 324 nm.

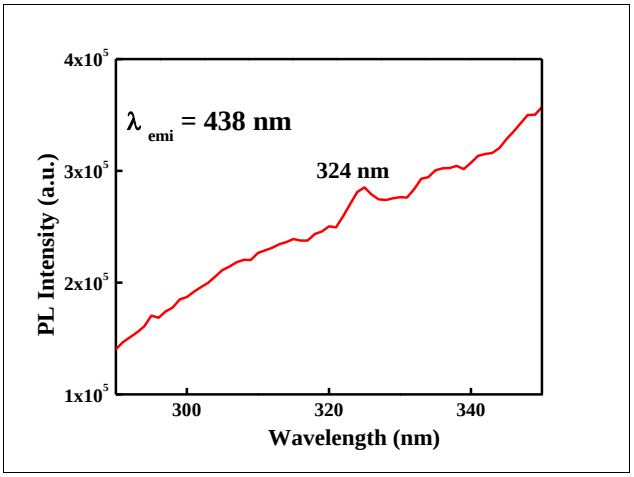

Fig 5B: PL excited spectrum of MoO_3: 3 NPs.

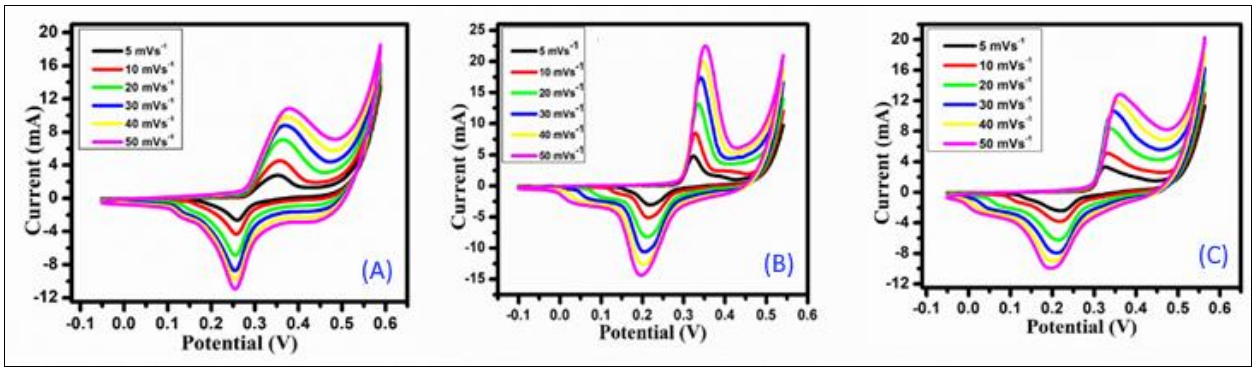

Fig 6: CV characteristics of the three samples (A) for HCL of 5%, (B) for HCl of 10% and (C) for HCl of 15%.

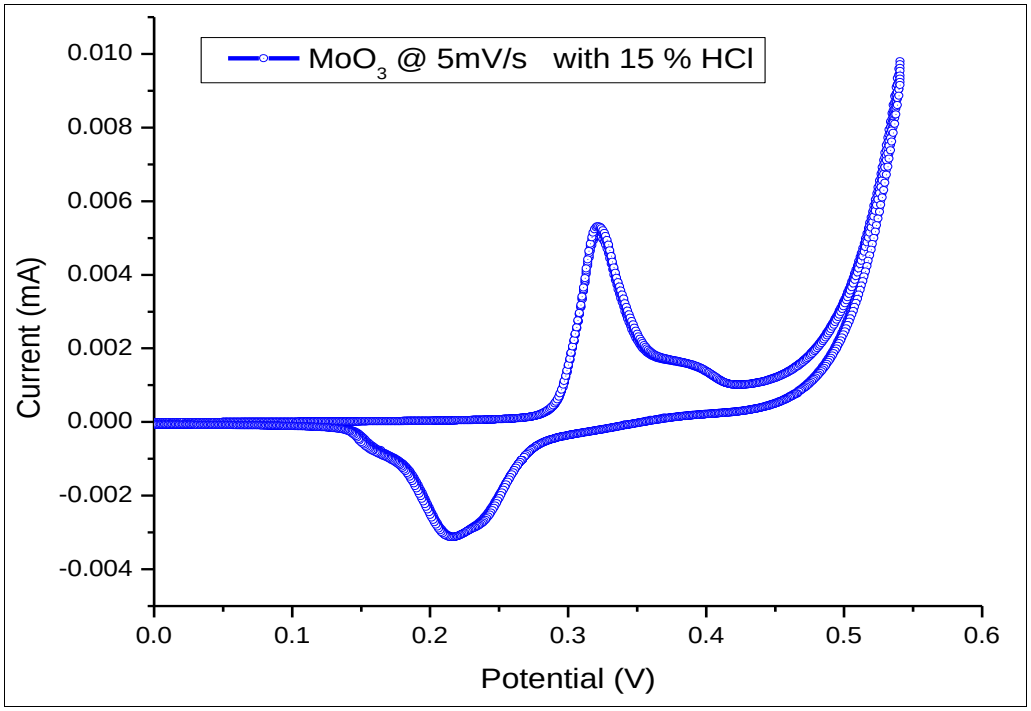

Fig 7: I-V Characteristics of a supercapacitor for the samples of 15% HCl concentration and applied voltage of 5 mV/s.

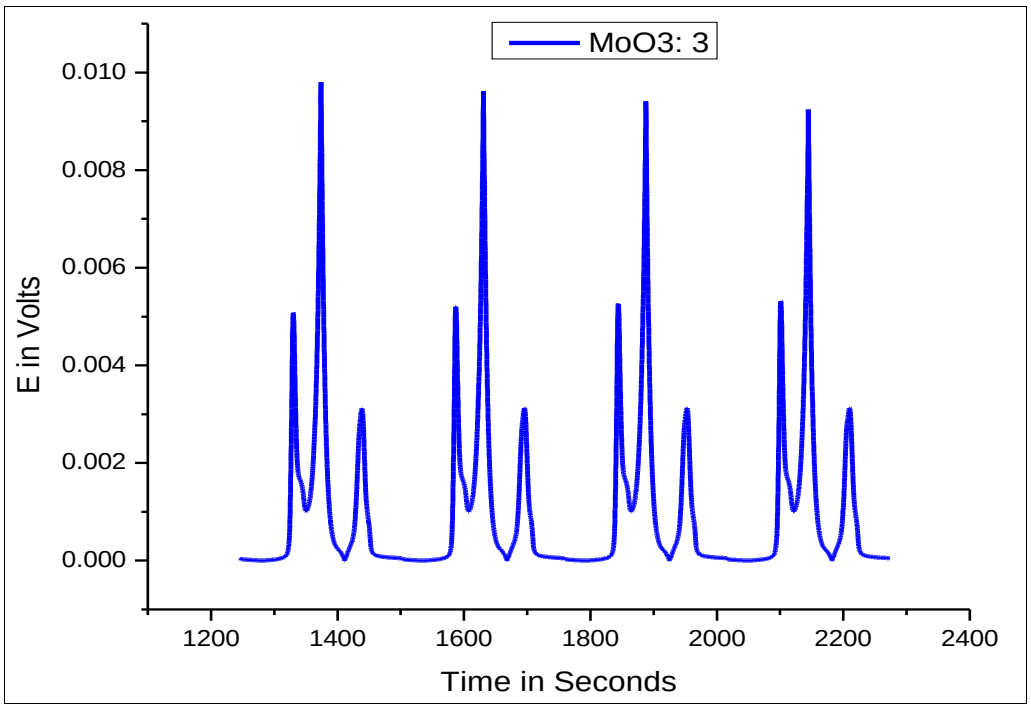

Fig 8: GCD plot of MoO_3:3 NPs (with 15% of HCl concentration).

Conclusions

MoO_3 Nanoparticles were prepared by sonochemical method with varied HCl concentration. PXRD results showed the nanoparticles of the crystallite size in 35 nm with rod shapes. SEM and TEM images showed the particles' agglomeration and also the clear rod-like structures, respectively confirming the nano-regime of the samples. UV-Vis studies, along with the Kubelka Munk function, showed that the samples are of wide band gap semiconductors, which vary with the change in HCl concentration. CV studies confirm that the prepared samples are good for supercapacitor applications based on the increased specific capacitance and the GCD results.

References

1. Mahalakshmi B, *et al.* exploring the potential of Ni-doped CuO nanoparticles as a promising electrode material for asymmetric supercapacitors. Journal of the Indian Chemical Society. 2025;102(2):101589.
2. Satpathy S, Das S, Bhattacharyya BK. How and where to use super-capacitors effectively: An integration of review of past and new characterization works on super-capacitors. Journal of Energy Storage. 2020;27:101044.
3. Iram F, Mustafa GM, Ali G, Ahmad H, Ramay SM, Iqbal Z, Atiq S. Transition metal (Zn, Mn, and Ni) incorporated CuO nanostructures for supercapacitor applications. Journal of Energy Storage.

2023;73:108829.
4. Taurino AM, Forleo A, Francioso L, Siciliano P. Applied Physics Letters. 2006;88:152111.
5. Yen B, Zheng Z, Zhang J, Gong H, Shan Z, Huang W, Yu T. Journal of Physical Chemistry C. 2009;113:20259-20264.
6. Li W, Cheng F, Tao Z, Chen J. Journal of Physical Chemistry B. 2006;110:119-124.
7. Hamwi S, Meyer J, Winkler T, Riedl T, Kowalsky W. Applied Physics Letters. 2009;94:253307.
8. Mariotti D, Lindstrom H, Bose AC, Ostrikov K. Nanotechnology. 2008;19:495302.
9. Pandeeswari R, Jeyaprakash BG. Biosensors and Bioelectronics. 2014;53:182-186.
10. Lunk HJ, Hartl H, Hartl MA, Fait MJ, Shenderovich IG, *et al.* "Hexagonal molybdenum trioxide" known for 100 years and still a fount of new discoveries. Inorganic Chemistry. 2010;49:9400-9408.
11. Noerochim L, Wang JZ, Wexler D, Chao Z, Liu HK. Journal of Power Sources. 2013;228:198-205.
12. Chen JS, Cheah YL, Madhavi S, Lou XW. Journal of Physical Chemistry C. 2010;114:8675-8678.
13. Huang L, Xu H, Zhang R, Cheng X, Xia J. Applied Surface Science. 2013;283:25-32.
14. Yao JN, Yang YA, Loo BH. Journal of Physical Chemistry B. 1998;102:1856-1860.
15. Yao DD, Field MR, O'Mullane AP, Kalantar-Zadeh K, Ou JZ. Nanoscale. 2013;5:10353-10359.
16. Sen UK, Mitra S. RSC Advances. 2012;2:11123-11131.
17. Sakaushi K, Thomas J, Kaskel S, Eckert J. Chemistry of Materials. 2013;25:2557-2563.
18. Fu Q, Chen J, Shi C, Ma D. ACS Applied Materials & Interfaces. 2013;5:6024-6029.
19. Niederberger M, Krumeich F, Muhr HJ, Muller M, Nesper R. Journal of Materials Chemistry. 2001;11:1941-1945.